Xu, Z., Juhlin, C., Gudmundsson, O., Zhang, F., Yang, C., Kashubin, A., Lüth, S. (2012): Reconstruction of subsurface structure from ambient seismic noise: an example from Ketzin, Germany. - Geophysical Journal International, 189, 2, pp. 1085—1102.

DOI: http://doi.org/10.1111/j.1365-246X.2012.05411.x

Geophysical Journal International

Geophys. J. Int. (2012) **189,** 1085–1102 doi: 10.1111/j.1365-246X.2012.05411.x

Reconstruction of subsurface structure from ambient seismic noise: an example from Ketzin, Germany

Zhuo Xu,[1,2] Christopher Juhlin,[1] Olafur Gudmundsson,[1] Fengjiao Zhang,[1] Can Yang,[1] Artem Kashubin[1,3] and Stefan Lüth[4]

[1] *Department of Earth Sciences, Uppsala University, Villavagen* 16, *Uppsala, Sweden. E-mail: zhuo.xu@geo.uu.se*
[2] *College of Geoexploration Science and Technology, Jilin University, Ximinzhu Street No.*6, *Changchun, China*
[3] *Schlumberger Cambridge Research, High Cross, Madingley Road, Cambridge, UK*
[4] *Helmholtz-Zentrum Potsdam Deutsches GeoForschungsZentrum (GFZ), Telegrafenberg,* 14473, *Potsdam, Germany*

Accepted 2012 February 4. Received 2012 February 4; in original form 2011 September 15

SUMMARY

Passive seismic interferometry is a new promising methodology for seismic exploration. Interferometry allows information about the subsurface structure to be extracted from ambient seismic noise. In this study, we apply the cross-correlation technique to approximately 25 hr of recordings of ambient seismic noise at the Ketzin experimental CO_2 storage site, Germany. Common source gathers were generated from the ambient noise for all available receivers along two seismic lines by cross-correlation of noise records. This methodology isolates the interstation Green's functions that can be directly compared to active source gathers. We show that the retrieved response includes surface waves, refracted waves and reflected waves. We use the dispersive behaviour of the retrieved surface waves to infer geological properties in the shallow subsurface and perform passive seismic imaging of the subsurface structure by processing the retrieved reflected waves.

Key words: Image processing; Inverse theory; Interferometry; Wave propagation.

1 INTRODUCTION

Seismic interferometry is a technique that enables the extraction of the seismic impulse response (Green's function) between two receivers by cross-correlation of wavefields recorded by the pair as if a virtual source were at one of the receiver locations. This method was pioneered by Claerbout (1968) when he showed that the 1-D reflection response of an arbitrary horizontally layered earth can be reconstructed from the autocorrelation of its transmission response. Seismic interferometry can be used in both passive seismic measurements and controlled-source seismic measurements. Active seismic interferometry, introduced by Gerard T. Schuster through the generalized correlation method for exploration-seismic data in 2000 (e.g. Schuster & Rickett 2000), comprises a new exploration-seismic processing methodology. One of the most exciting applications of seismic interferometry is the retrieval of Green's function from passive seismic data. The use of seismic interferometry to reconstruct the Green's function from ambient noise has been successfully applied in various fields of wave physics such as helioseismology, acoustics, ultrasonics, engineering, oceanography, seismology and geophysics. Historically, helioseismology was the first field used by solar physicists to measure ambient noise cross-correlation from recordings of random motions of the Sun's surface and then to infer information about its internal structure (Duvall *et al.* 1993; Gilles *et al.* 1997; Rickett & Claerbout 1999). In ultrasonics, Green's functions have been extracted from cross-correlation of diffuse thermal noise (Weaver & Lobkis 2001, 2003; Larose *et al.* 2004; Malcolm *et al.* 2004; Weaver & Lobkis 2004; Larose *et al.* 2006a). In seismology, surface waves have been reconstructed from retrieved Green's function by cross-correlating seismic noise at stations separated by distances of a few hundred metres to several hundred kilometres (Campillo & Paul 2003; Shapiro & Campillo 2004; Shapiro *et al.* 2005; Sabra *et al.* 2005b; Ritzwoller *et al.* 2005; Gerstoft *et al.* 2006; Larose *et al.* 2006b; Yao *et al.* 2006; Gudmundsson *et al.* 2007; Gouedard *et al.* 2008; Nunziata *et al.* 2009). In shallow underwater acoustics, direct and reflected wave fronts have been retrieved from ambient noise (Roux *et al.* 2004; Sabra *et al.* 2005a). In some applications, passive seismic interferometry has been used to image the Earth's subsurface structure based on noise recordings (Scherbaum 1987a,b; Daneshvar *et al.* 1995; Sheng *et al.* 2001, 2003; Shragge *et al.* 2006; Draganov *et al.* 2006, 2007, 2009).

Given that seismic interferometry is a process of generating virtual seismic responses by cross-correlating seismic observations at different receiver locations makes it an attractive method for construction of new deterministic seismic responses using only passive recordings of ambient seismic noise. In particular, retrieved surface waves can be further used to construct velocity profiles of the subsurface structure by inverting the dispersion characteristics extracted from the virtual data. Dorman & Ewing (1962) first attempted the inversion of dispersion curves to estimate shear wave velocities deep within the Earth. Retrieval of reflected waves is more challenging

because the amplitudes of reflected waves attenuate more rapidly with distance, and the distribution of the ambient noise sources is more strict compared to that for surface waves. Recently, however, reflected waves have also been retrieved from ambient seismic noise by seismic interferometry (e.g. Draganov *et al.* 2007, 2009). The retrieved reflection response can be used in many exploration applications in frontier fields, especially in areas with difficult terrain conditions and sensitive natural conditions. The retrieved seismic reflection response can also possibly be used for time-lapse passive imaging of subsurface structure as is routinely done in active seismic measurements (e.g. Lu *et al.* 2009). Passive seismic interferometry has the potential to become a relatively cheap, good-quality, convenient complement to active seismic surveys, especially in areas that are difficult towaves access.

In this study, we cross-correlate passive data that were recorded at night in conjunction with an active seismic survey in the Ketzin area, Germany. The data differ from most passive seismic surveys in that they were recorded using relatively high-frequency geophones (28 Hz). In spite of this, we show that we can retrieve surface waves, apparent refracted waves and reflected waves from the recorded ambient seismic noise by seismic interferometry. The retrieved surface waves are used to derive a shear wave velocity profile in the area. The retrieved reflected waves have been processed as common depth point (CDP) data to obtain structural images of the subsurface. These images have similarities with those obtained using the active seismic data that were recorded along the same lines.

2 PASSIVE SEISMIC DATA SET

2.1 Passive seismic field measurements and data acquisition

The passive seismic measurements were performed in 2011 February at the Ketzin CO_2 storage site (Förster *et al.* 2006; Martens *et al.* 2011) in conjunction with an active time-lapse survey to monitor the stored CO_2 (Fig. 1). The structure of the Ketzin site is well known from a 3-D surface seismic survey (Juhlin *et al.* 2007) that was performed prior to CO_2 being injected there. Sources of passive seismic energy may be natural (e.g. earthquakes), environmental (e.g. wind) or manmade (e.g. vehicles). Traffic along roads near the survey area may be viewed as surface wave sources, which were excited randomly in time. Passive data from two lines, Line 1 and Line 5 (Fig. 1), are analysed in this study. The acquisition geometry of Line 5 consisted of 62 geophones with a spacing of 24 m. Line 1 consisted of 39 geophones spaced also at 24 m intervals. The time sampling interval was 1 ms for both lines, and data were recorded over the same time intervals. The passive acquisition consisted of recording data continuously in 30 s panels (separate data files). As a result, ambient noise records were stored in 2976 noise panels over a period of approximately 25 hr, which were acquired during two nonconsecutive nights. In addition, during daytime, an active seismic survey was conducted along the same lines of geophones with spacing between source points of 12 m. The recording times of the active and passive recording did not overlap, so seismic energy generated during the active experiment could not contaminate the passive data studied in this work. Results from the active survey can be used for verification of the retrieved recordings from the passive seismic survey.

2.2 Ambient noise characteristics and pre-processing

Noise panels were visually inspected prior to cross-correlation. The frequency band between 2 and 30 Hz appeared to contain the most useful information even though 28 Hz geophones were used for the acquisition. In this frequency band, the noise panels show mainly random noise and propagating energy in the form of weak surface waves that are characterized as slightly dipping linear events. Some noise panels contain relatively strong surface waves generated by passing cars, where the hyperbolic shape of the events can be used to determine the car's position with respect to the receiver array at the time of recording. In most of the noise panels, propagating energy from deeper ambient noise sources is not obvious and is probably masked by the surface wave energy in the recordings, implying that retrieval of reflected waves from the noise may be more difficult compared to retrieval of surface waves. The most energetic part of the surface waves is concentrated below 14 Hz. Some of the noise panels contain visually identifiable body-wave noise with higher frequency content.

When retrieving the seismic response from the ambient seismic noise, we selected the energy between 2 and 30 Hz using a zero phase bandpass filter. To ensure that energy from all the ambient noise sources in the subsurface was equally weighted, all the noise panels were energy normalized before the cross-correlation procedure. Here, the trace energy normalization was a trace-by-trace process; the traces were scaled to have the same energy content. Fig. 2(a) shows a part of one 30-s ambient noise panel in the frequency band between 2 and 30 Hz. An example of an ambient noise panel containing surface waves generated by passing cars is shown in Fig. 2(b). Fig. 2(c) shows an example of an ambient noise panel containing identifiable body wave noise. The nearly horizontal arrivals on Lines 1 and 5 at nearly the same time (Fig. 2c) is strong evidence that we are indeed recording body-wave noise rather than surface waves propagating with a wave front parallel to Lines 1 and 5.

Further time domain normalization consisted of sign-bit signal conversion before the cross-correlation procedure. This method sets positive amplitudes to $+1$ and negative amplitudes to -1. Thereby, the unwanted influence of single transient signals and uneven illumination problems associated with the distribution of the most energetic arrivals is reduced by keeping only phase information (Derode *et al.* 1999; Campillo & Paul 2003). The sign-bit conversion was applied to the filtered, trace normalized, noise data and resulted in an overall improvement in the quality of the retrieved response compared to not applying it. The sign-bit conversion could have been applied directly to the filtered data without energy normalization step.

Another complication in passive seismic imaging is that the ambient noise sources should be evenly distributed in space for the entire wavefield to be recovered by cross-correlation. When a passive array is illuminated by an uneven distribution of noise sources it is necessary to average over the causal parts and acausal parts of the retrieved Green's function to obtain a result with optimal illumination (Draganov *et al.* 2007).

3 RETRIEVED RESPONSE FROM AMBIENT SEISMIC NOISE

3.1 Retrieval of surface waves and body waves from ambient noise measurements

To retrieve the response between a receiver pair in a passive array, seismic interferometry can be applied to the recorded ambient noise

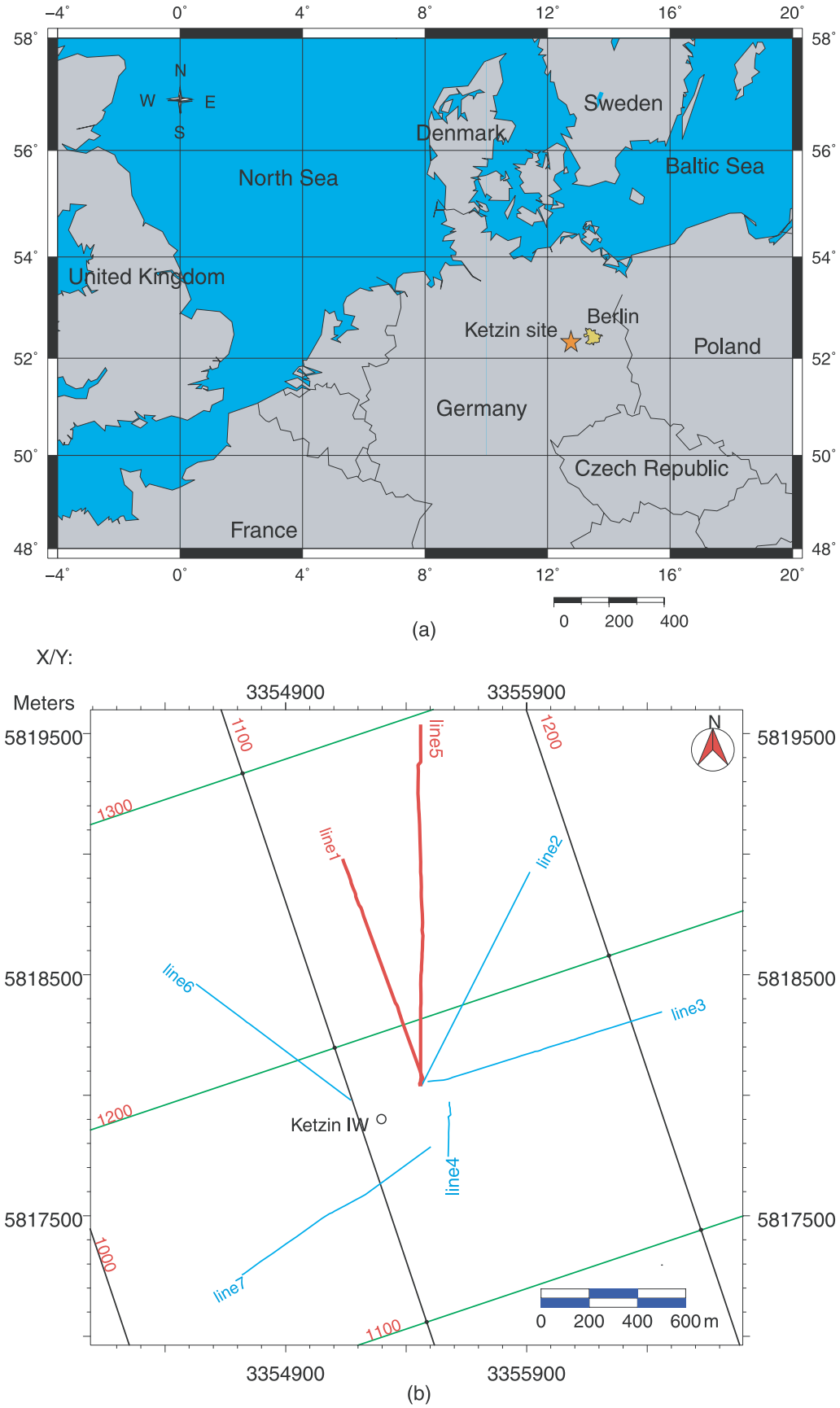

Figure 1. (a) Location of the Ketzin site, west of Berlin, Germany. (b) Location of the 2-D surface seismic lines (in total 7 lines), and the red lines are studied in this paper. The injection well (IW) at the Ketzin site is shown on the map as well. (Modified from Yang *et al.* 2010).

field using the relation (Wapenaar 2004; Draganov *et al.* 2009)

$$\{G_{p,q}(x_A, x_B, t) + G_{p,q}(x_A, x_B, -t)\} * S(t) = \langle v_p(x_A, -t) * v_q(x_B, t)\rangle. \quad (1)$$

On the left-hand side, $G_{p,q}(x_A, x_B, t)$ and $G_{p,q}(x_A, x_B, -t)$ denote the Green's function and its time-reversed version between two receiver positions x_A and x_B. These Green's functions are convolved with the autocorrelation of the source time function of the noise sources. The right-hand side denotes cross-correlation of the particle velocity recorded in the x_p and x_q directions ($p, q = 1, 2, 3$) at x_A and x_B, respectively. The angle brackets denote a spatial ensemble average, which is performed over all the ambient noise panels. It is assumed that the ambient noise sources are uncorrelated and randomly distributed in the Earth, and that they illuminate the passive array from all directions. With long ambient noise recordings, correlation results are retrieved at positive and negative time lags,

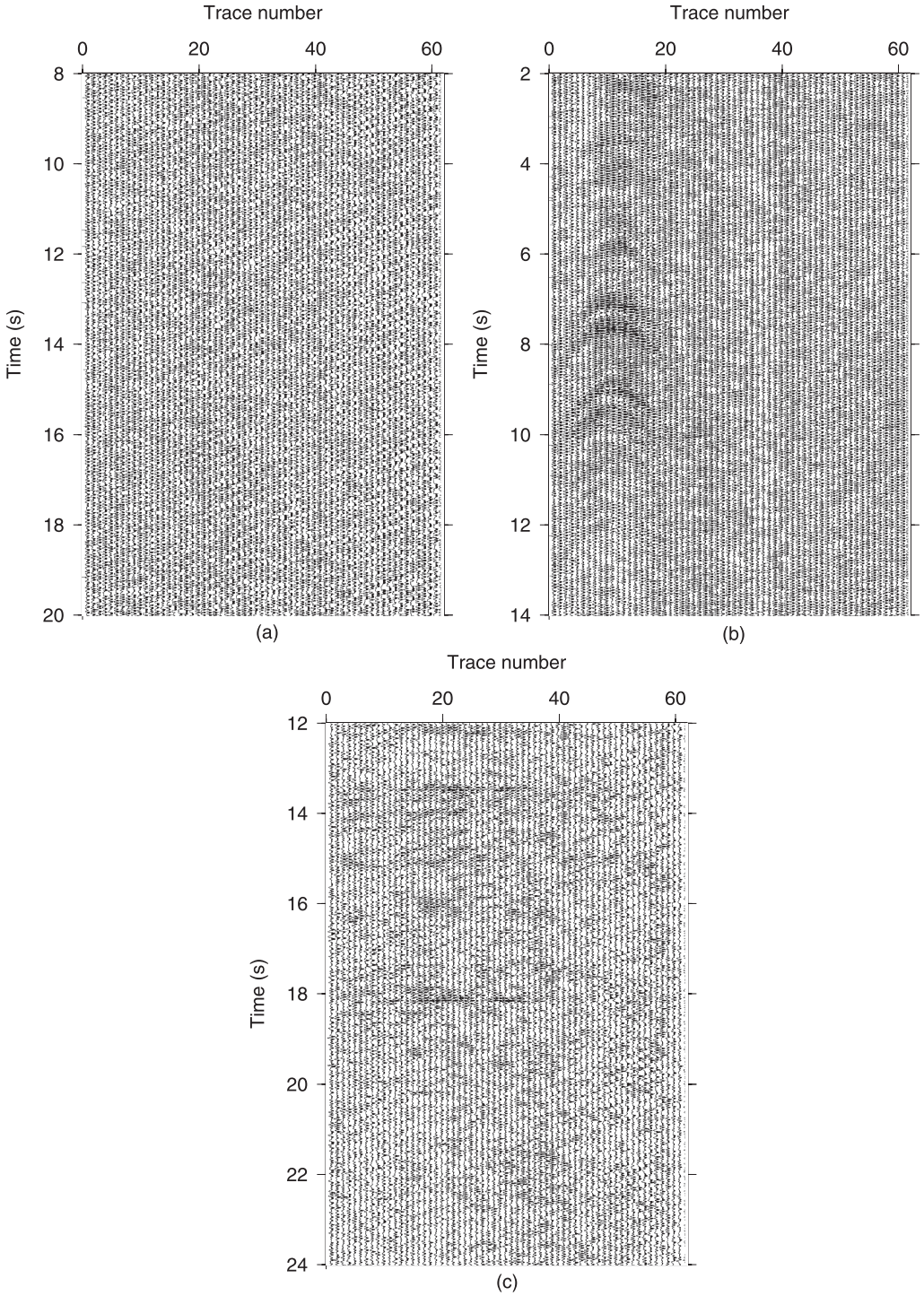

Figure 2. (a) Recorded ambient noise along Line 5 from a part of one of the raw noise panels with a bandpass filter between 2 and 30 Hz applied. (b) As in (a), but with clear surface waves generated by passing cars. (c) A part of one recorded ambient noise panel containing identifiable body-wave noise with a bandpass filter between 12 and 26 Hz applied.

corresponding to the two Green's functions on the left-hand side of eq. (1).

To obtain virtual source gathers from the ambient noise, we select a receiver position, extract the trace at that position and cross-correlate it with all other traces in the same noise panel giving a correlation panel. This was done for all noise panels, and all the correlation panels were then summed to generate a retrieved common source gather with the source located at the selected receiver position. We will refer to these as retrieved common source gathers. We repeated the cross-correlation procedure by choosing a virtual source at every receiver position along the receiver array. Every retrieved common source gather corresponds to the seismic response

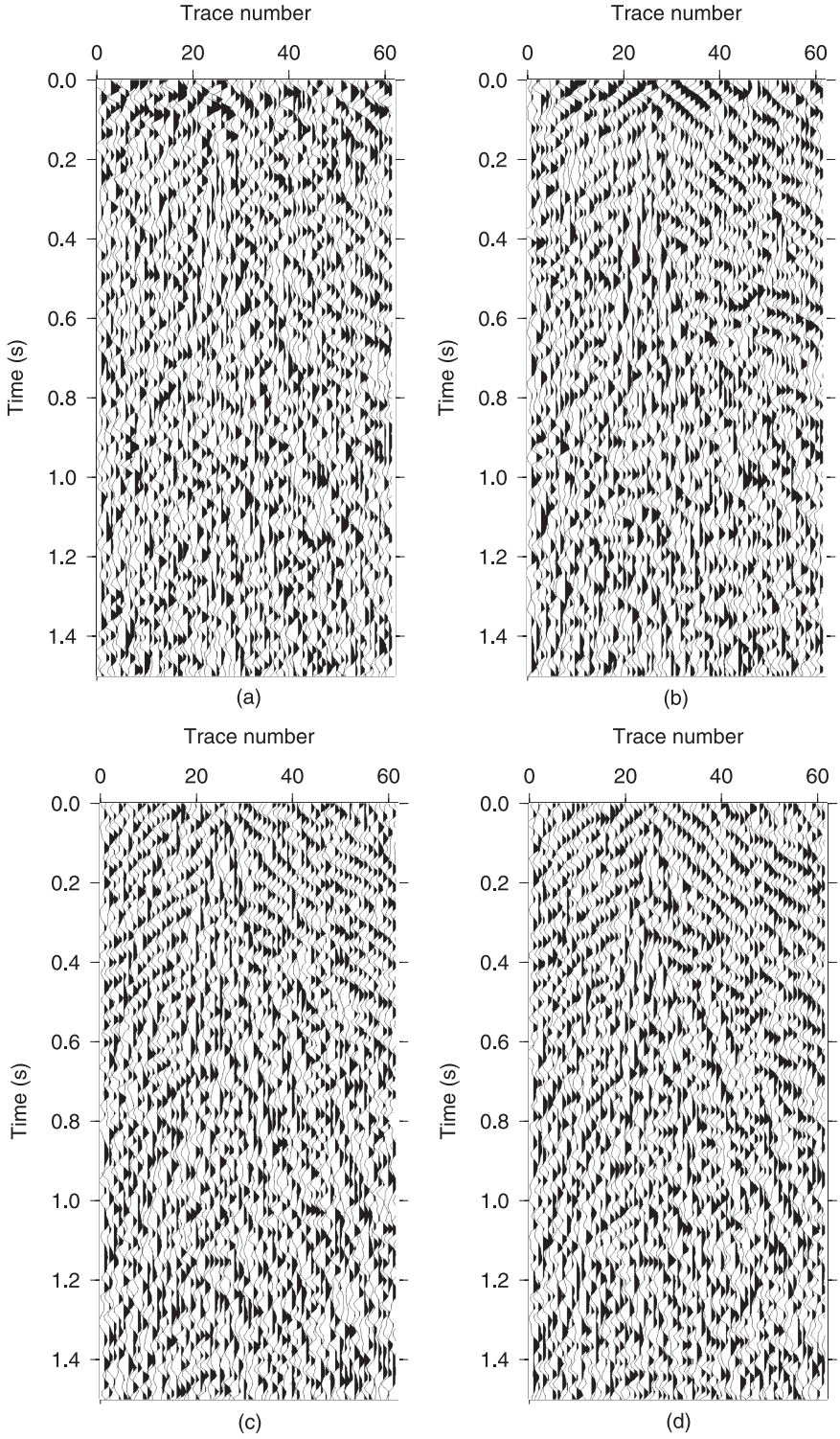

Figure 3. Retrieved seismic interferometry results from ambient seismic noise with a total recording time of: (a) 1 hr; (b) 5 hr; (c) 12 hr and (d) approximately 25 hr. The retrieved source is located at the 25th receiver position along Line 5.

of a source at the selected receiver position as observed by the receiver array. In total, we constructed 62 virtual common source gathers for Line 5 and 39 for Line 1. Each virtual source gather corresponds to a real physical seismic source as if it had been activated at that receiver position along the line.

The reconstruction of the Green's functions requires averaging over long time-series because longer ambient noise recordings record more information from subsurface noise sources and better fulfil the assumption that the ambient noise sources are uncorrelated, consequently improving the signal-to-noise ratio (SNR) and the coherence of the events in the retrieved common source gathers. Fig. 3 shows retrieved seismic interferometry results with a bandpass filter between 2 and 30 Hz applied, where the retrieved source is located at the 25th receiver position after cross-correlation of 1, 5, 12 and 25 hr of ambient noise recordings, respectively. As expected, the longer ambient noise recordings generate more coherent events in the retrieved common source gathers, especially the SNR of the retrieved interferometry results with 12 hr has been much improved compared to the results with 5 hr. In short, the quality of the response depends on the illumination characteristics of the ambient noise, the distribution of the ambient noise sources and the recording time length. However, only a minor improvement is achieved by lengthening the time-series from 12 to 25 hr (Figs 3c and d). For our data sets, the exploration scale of our ambient noise seismic measurements is not very large, the 25-hr noise appears sufficient for the retrieval of the most energetic events, namely the surface and apparent refracted waves. However, longer recording times than tens of hours may provide improvement for the retrieval of reflected waves in the virtual-source gathers. Note that an important constraint and cost of the passive seismic method is the length of time equipment must be in the field: the shorter the time the field measurements are performed, the lower the investment costs to acquire the data and the faster the computations to generate the virtual source gathers.

Dispersive surface waves can be easily identified in our retrieved common source gathers. A series of dipping coherent events correspond to the fundamental mode surface wave and possibly higher-mode surface waves (Rayleigh waves). To enhance the frequency content associated with the surface waves, we applied spectral equalization between 2 and 14 Hz (Fig. 4a). Comparison of one of the retrieved common source gathers with an active source gather recorded from the active source closest to the location of the retrieved source position shows that surface wave energy is stronger and more coherent in the retrieved source gather (Fig. 4). Note that the active source gather was bandpass filtered between 2 and 14 Hz to match the frequency content of the retrieved response. Even after this bandpass filter, surface waves in the active source gathers are less clear. The active source surface waves have a similar apparent velocity as the virtual source surface waves. Retrieved good quality surface waves from our ambient noise data compared to surface waves from the active source measurement are indicated by the red ellipses in Fig. 4. Consistent with previous work by other researchers at other sites, the seismic interferometry method works well at Ketzin for surface wave retrieval. The dispersive behaviour of the surface waves will later be used to characterize the shallow-subsurface structure in the area.

Aside from the retrieved surface waves, also what appears to be clear virtual refractions, some signs of reflected waves and spurious waves are present in our retrieved common source gathers. The theory of virtual refractions was recently presented and developed (Dong *et al.* 2006; Mikesell *et al.* 2009; Nichols *et al.* 2010), where the mechanism generating virtual refractions is different from that which generates reflected waves, as will be shown later. The quality of the retrieved surface and body waves is partly controlled by the distribution of the ambient noise sources and the characteristics of the recorded ambient seismic noise. In general, retrieved surface waves come mainly from sources at or near the surface while retrieved reflected waves result from recording body-wave-dominated noise from sources located in the deeper subsurface. Noise sources near the surface are relatively active in this area, implying that retrieval of surface waves from the ambient noise should be efficient.

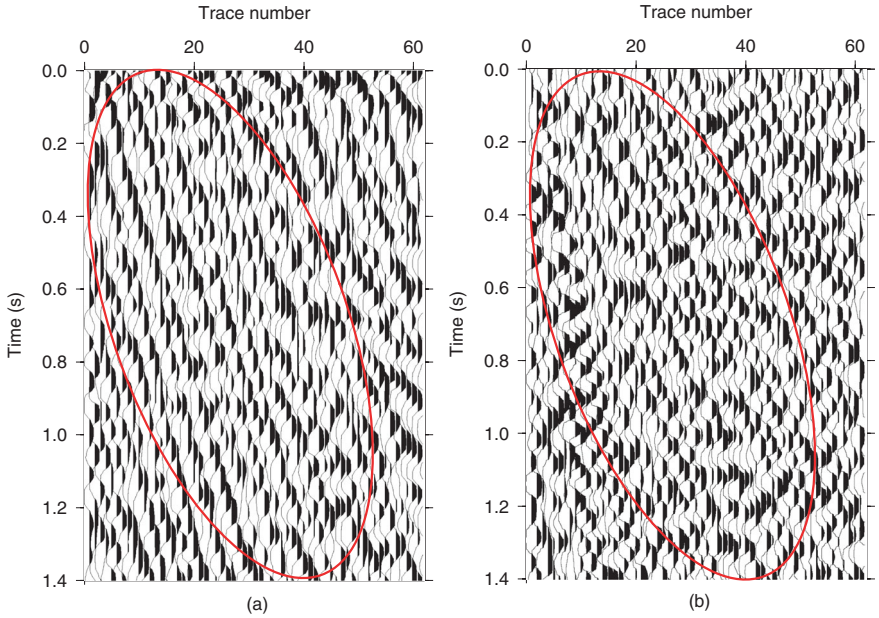

Figure 4. (a) Retrieved common source gather with a virtual source located at the position of the third receiver (Line 5). The source gather is dominated by surface waves after spectral equalization between 2 and 14 Hz. (b) Active common source gather with a source located near the same receiver position after bandpass filter between 2 and 14 Hz. The matching part of the surface waves is indicated by red ellipses.

Since surface waves dominate the raw ambient noise data and body waves have lower amplitudes and attenuate more rapidly compared to surface waves, it is natural to expect that the retrieval of reflected waves will be more difficult.

To improve the clarity and coherency of retrieved body waves we need to suppress the surface waves and enhance the body waves. We selected the frequency band between 12 and 26 Hz with spectral equalization for further processing. Fig. 5 shows a comparison between reflected waves in a retrieved source gather and an active source gather, where the active source gather is close to the same location as the retrieved source gather. The active source gather has also been bandpass filtered between 12 and 26 Hz to match the frequency content of the retrieved source gather. In general, the frequency content of the retrieved body waves from the passive seismic data is lower than the frequency content of the body waves from the active seismic survey at the same locations. We observe clear and consistent reflected waves in the retrieved common source gathers where the reflected waves are characterized as slightly hyperbolic coherent events with high apparent velocities. However, the velocities of the retrieved apparent refracted waves at far offsets in the retrieved common source gathers are higher than expected. Since we have many sources in the stationary-phase regions, these virtual refractions with higher apparent velocities for the distant offsets should be from deeper layers, as expected. Aside from the virtual refractions, other obvious artefacts are also present in the retrieved common source gathers. Especially obvious is the energy appearing before the theoretical onset of the first arrival in Fig. 5(a). These spurious waves are caused by a non-ideal spatial distribution of ambient noise sources in the subsurface and are correlation artefacts that did not destructively interfere during the summation process.

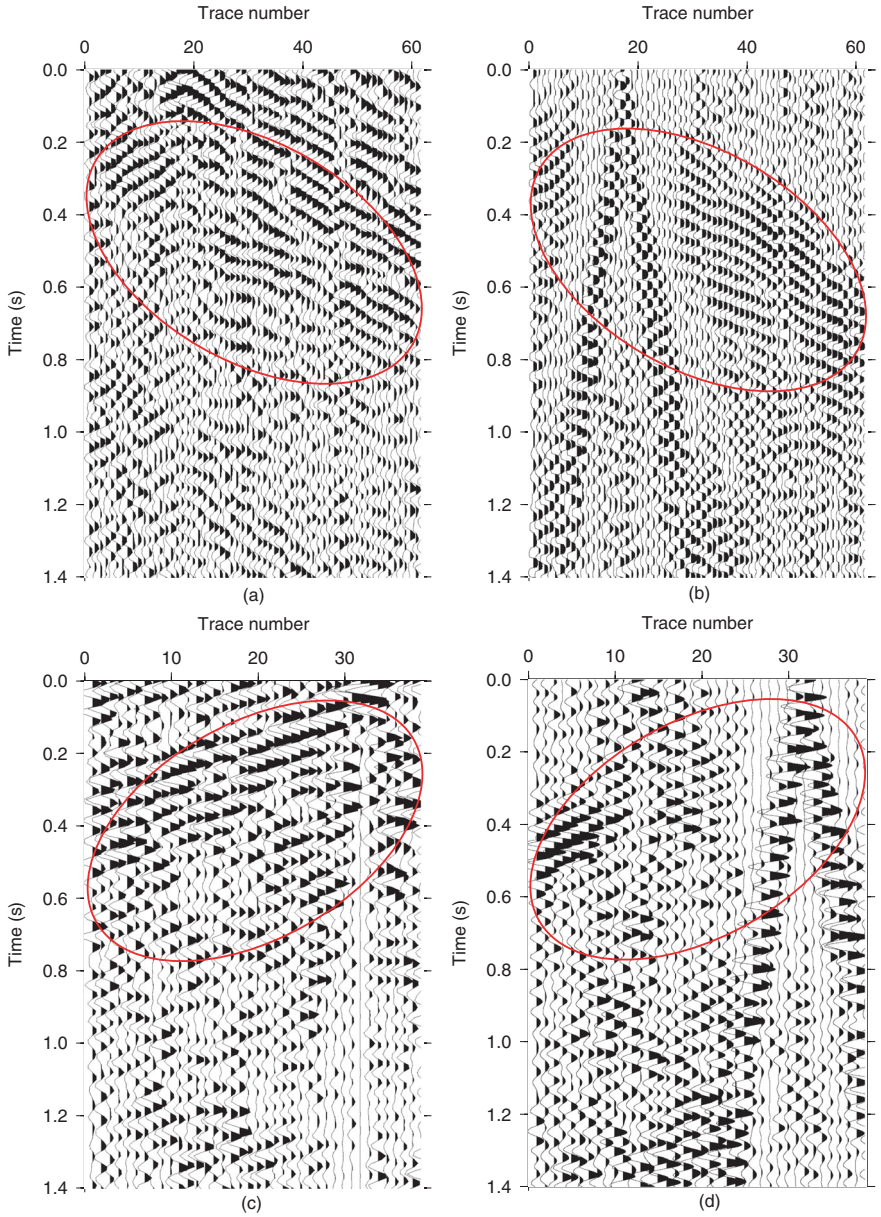

Figure 5. (a) Retrieved common source gather with the retrieved source located at the position of the 18th receiver (Line 5). The retrieved gather contains mainly body waves after spectral equalization between 12 and 26 Hz. (b) Active common source gather with a source located near the same receiver position (Line 5) after bandpass filter between 12 and 26 Hz. (c) As in (a), but with the retrieved source located at the position of the 32nd receiver (Line 1). (d) As in (b), but with a source located near the same receiver position (Line 1).

3.2 The virtual refractions and artefacts

To illustrate the virtual refractions in the retrieved common source gathers, we performed forward modelling based on the known subsurface structure in this area (Yordkayhun *et al.* 2007). The subsurface structure in this area can be approximated by horizontal layers. The synthetic velocity model used is shown in Fig. 6(a). The acquisition geometry consisted of 101 shots, which were randomly distributed between depths of 150 and 466 m (in the second and third horizontal layers) and evenly distributed at 10 m intervals in the horizontal direction, and 101 receivers that were evenly placed at an interval of 10 m on the surface. The synthetic common source gathers were modelled using a 2-D finite difference programme (Juhlin 1995). We used the transmission response of all the subsurface gathers to reconstruct a common source gather at the surface. At the same time, we modelled a common source gather with a source on the surface for comparison. Receiver data from the transmission response were cross-correlated with one another and summed, as described earlier for the passive data, to retrieve virtual source gathers at the surface. An example of a retrieved common source gather with the retrieved source located at the midpoint of the receiver array is shown in Fig. 6(b). The directly modelled common source gather with the source located at the same position at the surface is shown in Fig. 6(c). There is a phase difference in the source wavelet between the directly modeled and the retrieved common source gathers because of the change of source wavelet during the cross-correlation process (Snieder 2004; Wapenaar & Fokkema 2006). By comparing the retrieved body-wave events and the directly modelled body-wave events we find that we can fairly well reconstruct the body-wave response. The traveltimes of the reflected waves match well, but the direct waves in the retrieved common source gathers cannot be recovered correctly when all the sources are distributed at depth and no sources are found in the stationary-phase regions, which are at and near the surface (Wapenaar & Snieder 2007; Forghani & Snieder 2010). The spurious coherent event travelling at the velocity of the deeper layer that crosses the origin and arrives before the theoretical direct wave is the virtual refraction. The virtual refraction is a direct result of violating the far-field approximation of the Green's function. Unlike a true refraction, the virtual refraction intersects the origin. We also

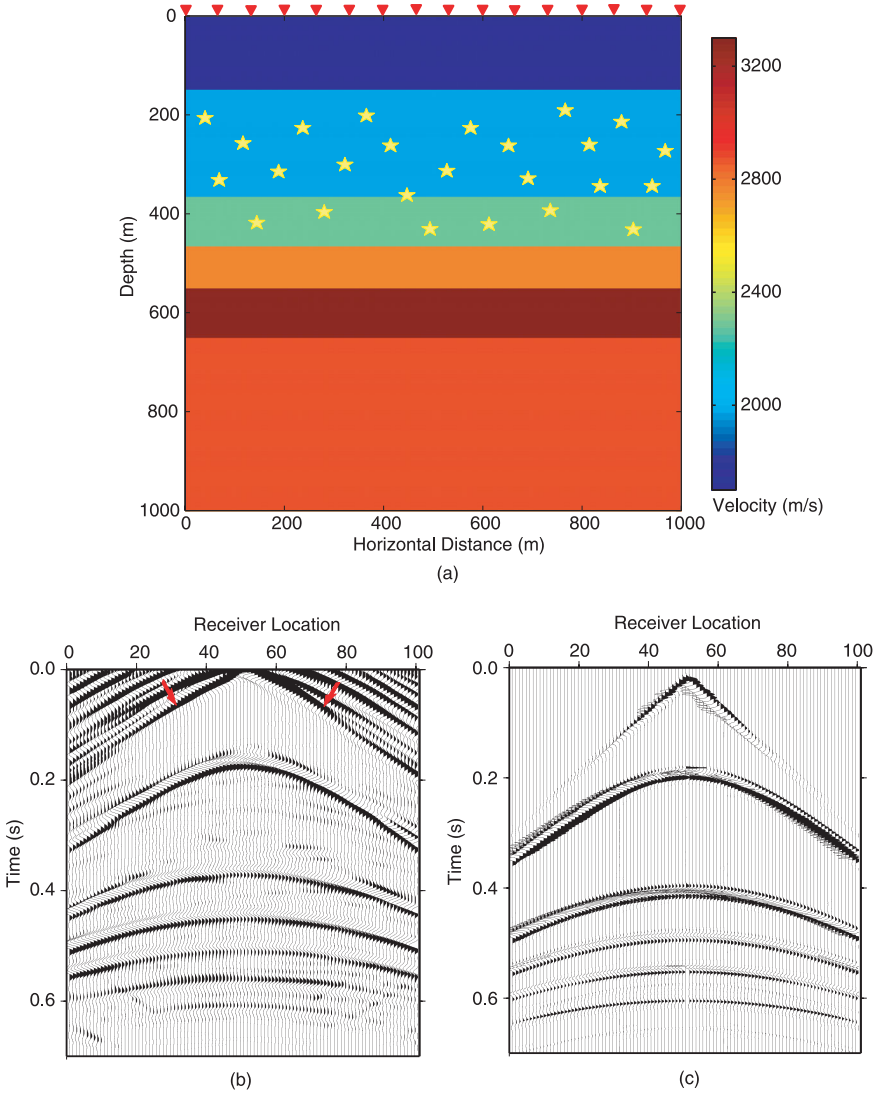

Figure 6. (a) Velocity model based on geological information of the subsurface at Ketzin. (b) Retrieved common source gather with the virtual source located at the middle of the receiver array. The virtual refraction indicated by arrows. (c) Directly modelled common source gather for a source located at the surface in the same position as the virtual source gather in (b).

interpret virtual refractions in the passive-source data as mentioned above with Fig. 5(a) corresponding to the passive response and Fig. 5(b) to the active response. In addition to the virtual refraction, we also observed other spurious linear waves that do not cross the origin in the early time part of the retrieved common source gathers, and are probably caused by the practical limitation of a finite number of sources. Therefore, they do not destructively interfere in the summation process. The same is true for the spurious waves in the real retrieved common source gathers. Our modelling exercise shows that deeper noise sources can generate virtual refractions that are similar to the ones that we observe in our passive data.

3.3 Common-offset-stack gathers

To produce a more robust retrieved response, we sorted all the retrieved common source gathers into common offset gathers and then stacked the latter to generate a single stacked common source gather. This stacking process effectively suppresses noise from different sources and consequently improves the SNR and the consistency of the events in the retrieved results. However, this comes at the cost of loosing lateral resolution. This stacking process assumes that the structure below the array is 1-D. The stacking process not only improves the coherency of the surface waves and the apparent refracted waves, but also the reflected waves are now more obvious (Fig. 7a). To further enhance the different wave types, the same spectral equalization was applied to the surface and body waves as before, respectively (Figs 7b and c). In Fig. 7(b) we note that a clear hyperbolic event with an apex at around 0.2 s, and with a high-velocity moveout marked by an arrow, is a retrieved reflection arrival with a low-frequency content, that is, in the frequency band of the primary surface wave energy.

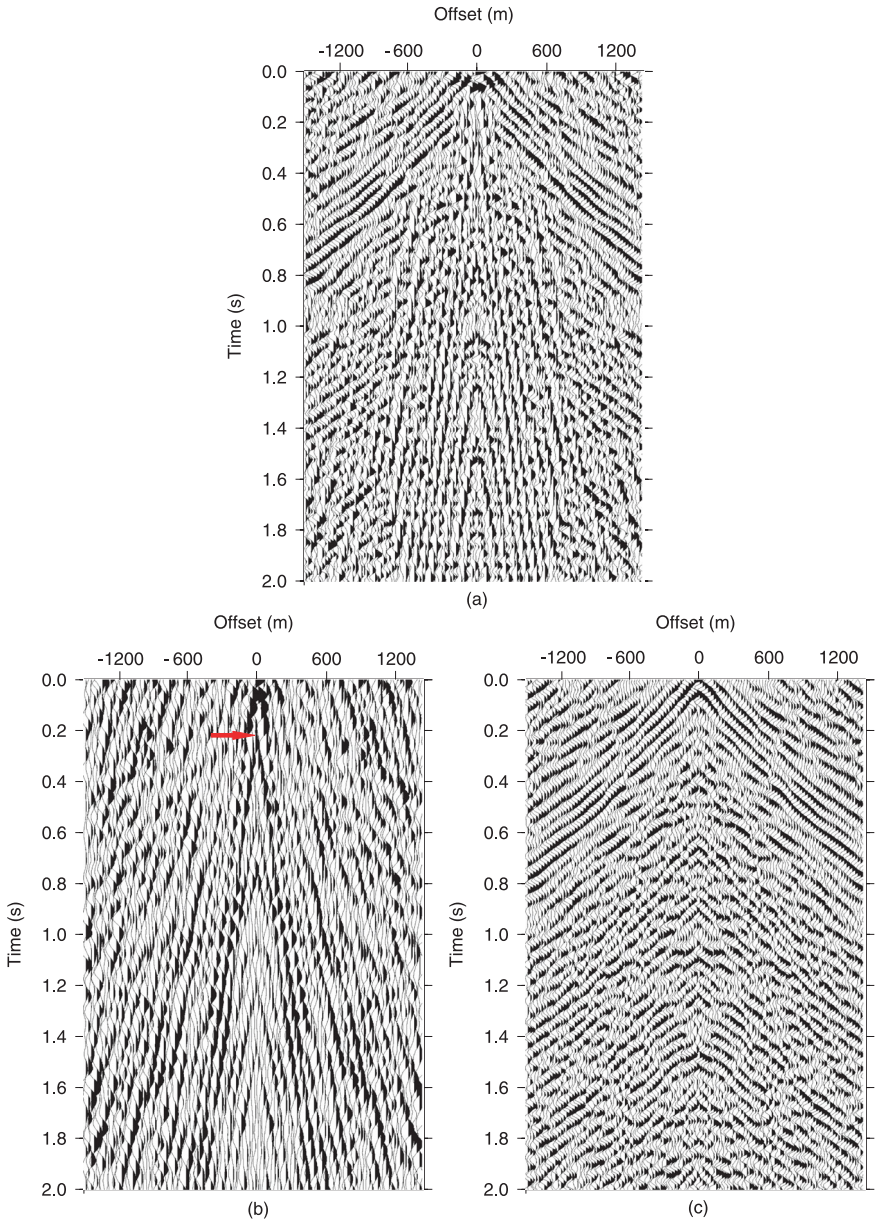

Figure 7. (a) Stacked common source gather generated by stacking common offset gathers retrieved from the ambient seismic noise after spectral equalization between 2 and 30 Hz. (b) As in (a), but dominated by surface waves due to spectral equalization between 2 and 14 Hz. (c) As in (a), but dominated by body waves due to spectral equalization between 12 and 26 Hz.

4 SURFACE WAVE ANALYSIS AND ESTIMATION OF A SHEAR WAVE VELOCITY PROFILE

Rayleigh waves are surface waves composed of interfering *P* and *SV* waves that propagate along the Earth's free surface. A main characteristic of surface waves is their dispersive behaviour when the velocity changes with depth. Dispersion curves for a layered earth model are a function of four Earth parameters: compressional wave (*P* wave) velocity, shear wave (*S* wave) velocity, density and the layer thickness of each geological layer. *S*-wave velocity is the dominant parameter of the four. Therefore, by analysing the dispersive behaviour of Rayleigh waves observed in recorded seismic data, it is possible to obtain a near-surface shear wave velocity (V_s) profile and construct a model of the shallow subsurface structure.

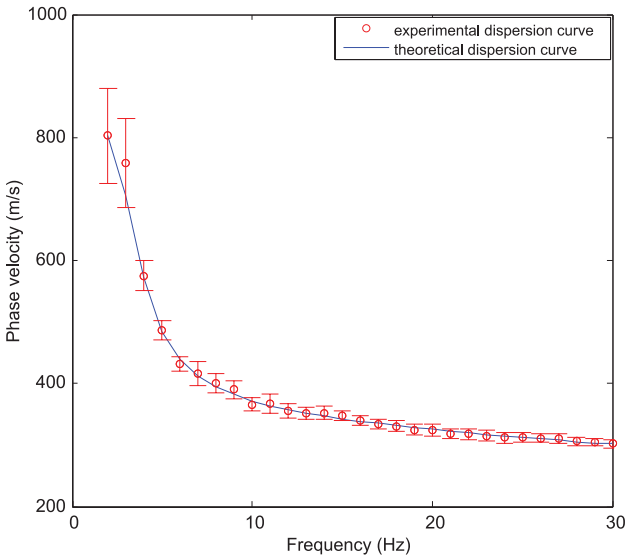

Figure 8. The experimental dispersion curve calculated from the retrieved data set and the theoretical dispersion curve.

One of widely available surface wave analysis techniques used to estimate dispersion curves is the spectral analysis of surface waves (SASW) method (Nazarian *et al.* 1983). The Rayleigh wave dispersion curves are generated on the basis of the analysis of phase–velocity differences between receivers. For each receiver pair with spacing dx, the time delay dt for a given phase velocity C_f of the surface wave as a function of frequency f is

$$C_f = \frac{\mathrm{d}x}{\mathrm{d}t}. \tag{2}$$

Such an analysis produces a set of dispersion curves (C_f vs. f) for each receiver pair. These curves are assembled together to form a composite dispersion curve.

We used Rayleigh waves from the retrieved common-offset stack panel as input data to calculate the experimental surface wave dispersion curve. However, our field configuration of receivers, that was used to record the ambient noise, was not specifically designed for recording the ground roll, so the consistency of the phase velocities of our retrieved surface waves is quite variable. The surface waves in the reconstructed gathers are spatially aliased at the highest frequencies. To obtain a reliable dispersion curve for our data, the selection of receiver pairs is critical. To avoid effects of near- and far-offset configurations, we chose receiver pairs that were located in the central part of the receiver array. The spacing between the receiver pairs was increased for analysis of longer wavelengths and decreased for shorter wavelengths. We used good-quality records to estimate the dispersion curves for each receiver pair and then assembled them together to obtain one composite dispersion curve. The experimental surface wave dispersion curve with error bars from Line 5 is presented in Fig. 8. The error bars are estimated from the distribution of measurements at individual frequencies. They illustrate that the uncertainty of the dispersion curve increases with decreasing frequency, implying that uncertainty increases with increasing depth.

We used the surface wave code in the package named Computer Programs in Seismology (CPS) to calculate theoretical dispersion curves (Fig. 8). CPS is a collection of FORTRAN and C routines developed and complied by Herrmann & Ammon (2002). It can be

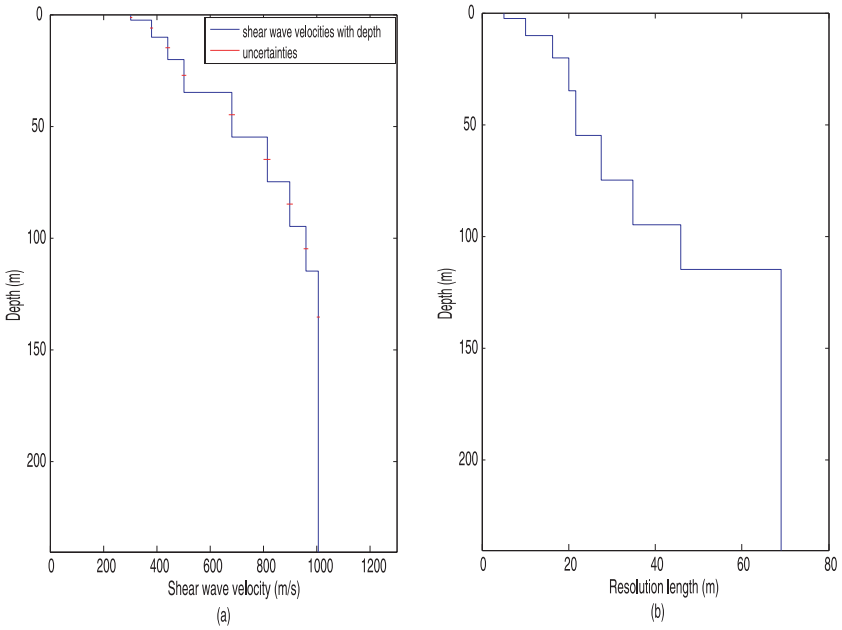

Figure 9. (a) The resulting shear wave velocity profile. (b) The resulting resolution length of surface wave profile.

Table 1. Tabulated model profile.

Layer number	Thickness (m)	*P*-wave velocity (m s^{-1})	*S*-wave velocity (m s^{-1})	Poisson's ratio (gm cc^{-1})
1	5	606.8	303.6	1.886
2	10	761.4	380.6	1.964
3	10	880.2	440.1	2.015
4	20	1009.9	504.8	2.063
5	20	1361.0	680.8	2.166
6	20	1621.3	810.8	2.227
7	20	1789.5	894.8	2.261
8	20	1910.0	955.2	2.284
9	Half-space	2006.5	1003.2	2.301

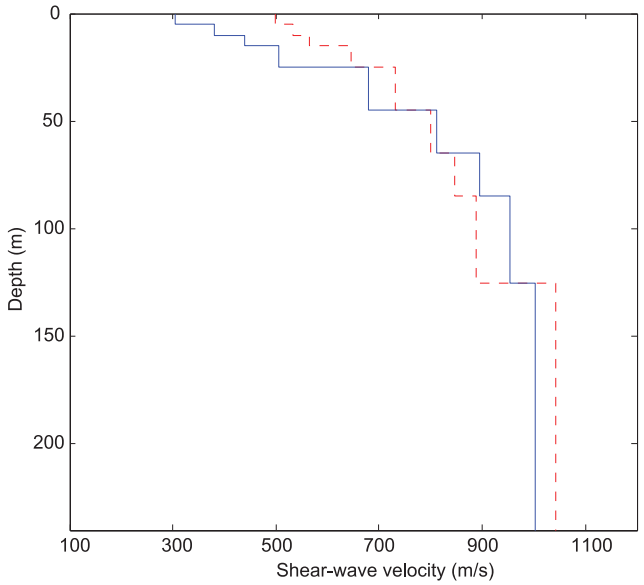

Figure 10. The shear wave velocity profile estimated from the surface wave inversion of the passive seismic data set (blue solid line) and the traveltime tomographic inversion of the active seismic data converted to shear wave velocities using a V_p/V_s ratio of 2 (red dashed line).

used to calculate the phase–velocity dispersion curves of surface waves for a given shear velocity profile and to derive the shear wave velocities by inverting the dispersion curve of the surface waves. A theoretical dispersion curve can be generated for an assumed velocity profile. This profile should contain a sufficient number of layers to define the variation of material properties at a site. Based on *a priori* geological information combined with previous analyses of the subsurface medium, we set the starting model as a nine-layer model with *P*-wave velocity, *S*-wave velocity and density specified for each layer corresponding to *a priori* parameters of the deepest layer of the starting model, these being 2000 m s^{-1}, 1000 m s^{-1} and 2.1 g cc^{-1}. After calculation of the dispersion curves for the initial model, the inversion process estimates an updated shear wave velocity profile from the misfit between the predicted and experimental dispersion curves. This process is then iterated until the misfit is satisfactory. The resulting shear wave velocity profile with estimated uncertainties and resolution lengths is shown in Figs 9(a) and (b), respectively. The resolution length is estimated from the resolution matrix of the final linear iteration of the inversion. The resulting material parameters listed in Table 1 are layer thickness, density, *P*-wave velocity and *S*-wave velocity for each geological layer, respectively. The resulting shear wave velocity profile from the inversion of the Rayleigh waves of the passive data set is shown as a blue solid line in Fig. 10 (same as blue line in Fig. 9a).

We compared the near-surface shear wave velocities from the retrieved surface wave data with an *S*-wave velocity model derived from the *P*-wave velocities based on first arrival traveltime tomography of the active data according to *a priori* information on the V_p/V_s ratio that is assumed to be 2. The active source gathers contain strong ground roll signals on the near-offset traces, while the far-offset traces have interference from ambient noise. Therefore, a 200–600 m offset window was used to pick first arrivals to avoid picking incorrect phases. Traveltime tomography was performed using the velocity model in Fig. 6(a) as the starting model. A *P*-wave velocity profile was then computed as an along-profile average of the tomographic result. Finally, an *S*-wave velocity

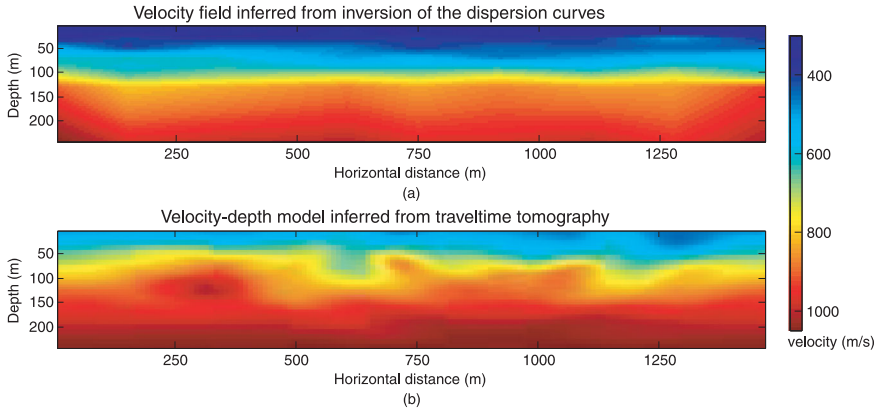

Figure 11. (a) Velocity field along Line 5 inferred from inversion of the dispersion curves for the passive data set and (b) the velocity–depth model inferred from traveltime tomography from the active data set along Line 5.

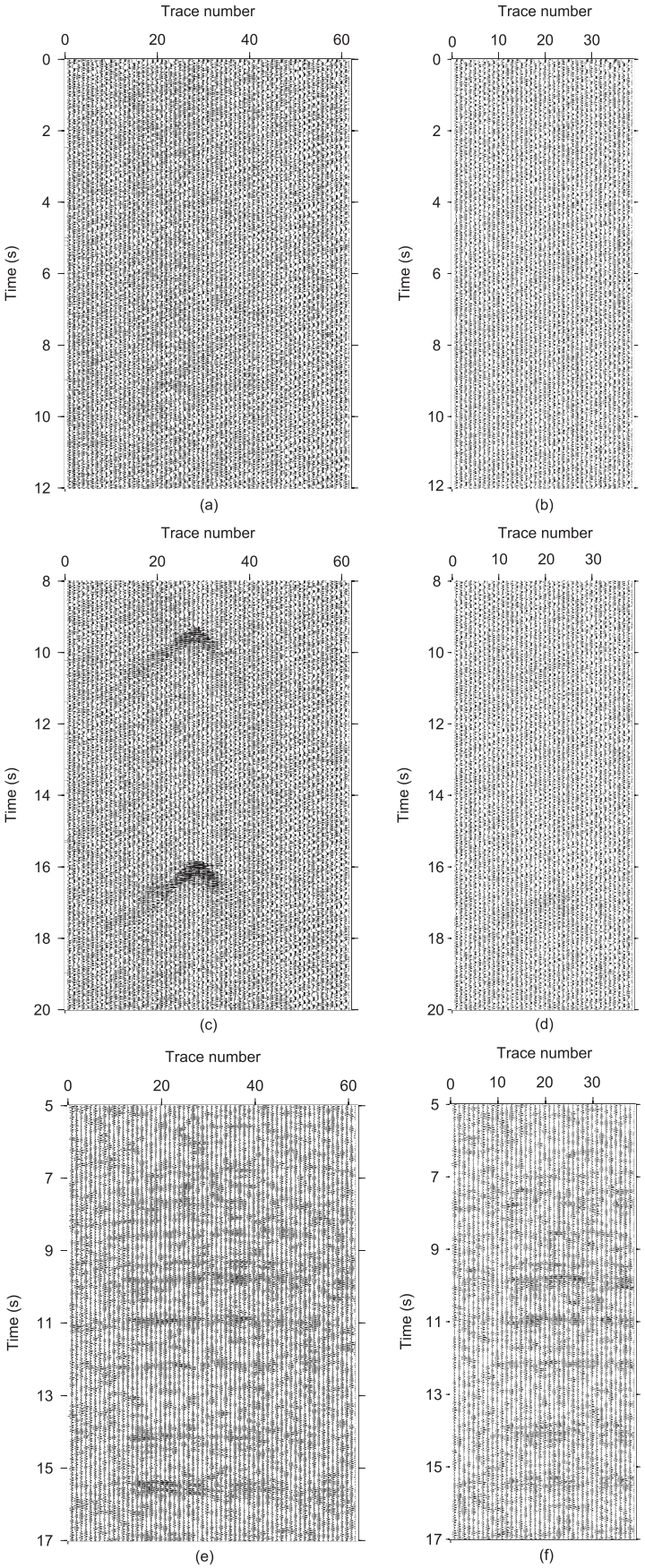

Figure 12. Examples of noise panels from Line 5 (a) compared with the same noise panels from Line 1 (b). (c,d) As in (a) and (b), but with surface waves generated by passing cars. (e,f) As in (a) and (b), but containing body-wave noise.

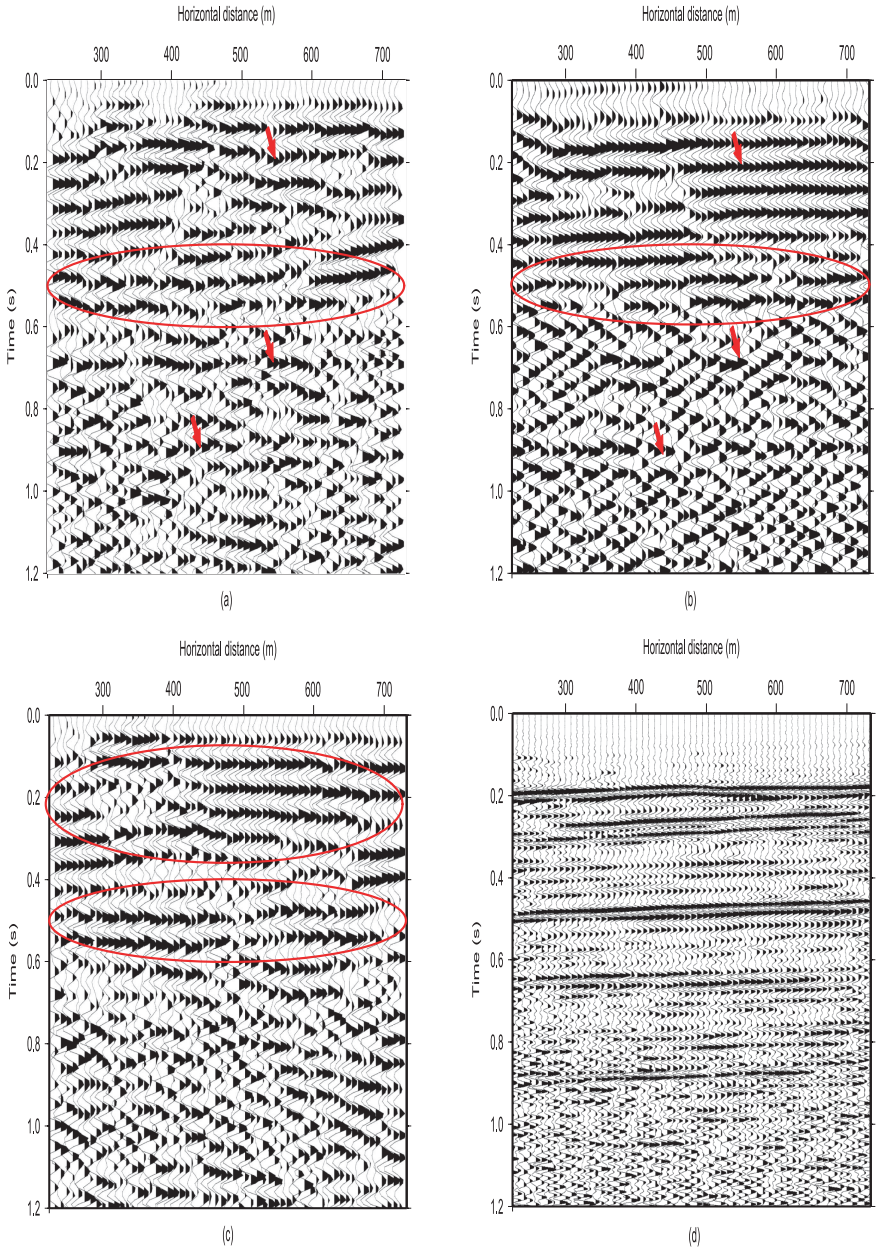

Figure 13. Stacked seismic sections obtained along Line 1 from: (a) the retrieved common source gathers from the passive measurements, (b) the common source gathers from the low-frequency content of the active source survey, (c) the retrieved common source gathers using only noise panels containing identifiable body-wave noise and (d) the common source gathers from the full bandwidth active source survey.

structure was estimated from the calculated *P*-wave velocities using a value of 2 for the V_p/V_s ratio. The estimated tomographic *S*-wave velocity structure is shown as a red dashed line in Fig. 10. The deeper parts of the shear wave profile from the passive surface wave data agree well with the calculated tomographic shear wave velocities from the active source traveltime data. However, at shallower depths, the inverted shear wave velocities from the ambient noise data are lower. This discrepancy can be attributed to the higher resolution of the surface wave inversion at shallower levels. If *P*-wave velocities from longer-offset surveys in the area (Yordkayhun *et al.* 2007) are converted to *S*-wave velocities assuming a V_p/V_s ratio of 2, then the deeper inverted *S*-wave profile agrees well with this active source traveltime data. The uppermost 100 m in the area consists mainly of glacial sands (Yordkayhun *et al.* 2009a). The compaction of these sands with depth will result in increases in both the *P*- and the *S*-wave velocity. When a tomographic inversion of active source *P*-wave data is preformed, a strong gradient is observed in the *P*-wave velocity profile in the uppermost 50 m over much of the area (Yordkayhun *et al.* 2009b). A similar increase may be expected for the *S*-wave velocity.

As a further comparison between the passive data and the active source data, we generated a 2-D model from the passive surface wave data and compared this with the 2-D calculated *S*-wave velocity model generated by converting the *P*-wave velocity traveltime tomography model (Fig. 11). We selected several good-quality surface wave responses from the retrieved common source gathers along the whole survey line as input to calculate a 2-D velocity–depth profile. To match the resolution of the velocity–depth model from traveltime tomography, we used a linear interpolation method to smooth our velocity–depth profile derived from the passive surface wave data,

so that it has the same resolution length as the traveltime tomography result, that is 5 m. The final velocity–depth models from the active and passive seismic data sets are similar in the deeper parts, but, again, for the uppermost layers the velocities from the surface wave inversion are lower than velocities from the traveltime tomography (Fig. 11). Velocities in both velocity–depth models increase slowly with depth. Given that the surface waves best exhibit themselves in the 2–14 Hz range the deployment of 28 Hz geophones was probably not ideal for inferring deeper velocity information. Deployment of lower-frequency geophones at a tighter spacing might have allowed a more detailed model to be extracted from the data, both shallower and deeper.

5 REFLECTION SEISMIC IMAGING

Retrieval of reflected seismic waves is challenging work in our study area because surface waves dominate the ambient noise, thus reflected waves are masked in the recorded ambient noise. Although we have retrieved clear reflected waves in some of the reconstructed interferometry gathers from the passive seismic survey of Line 5, not all the retrieved common source gathers contain identifiable and clear reflected waves. Initial processing of these common source gathers, where all gathers were input without any selection criteria (brute force processing), to a common-depth-point (CDP) stack along Line 5 did not produce a satisfactory result. Therefore, to further test the feasibility of passive imaging in our study area we used ambient noise from Line 1 to reconstruct virtual source gathers along that line. Examples of ambient noise panels recorded at the same moment and in the same frequency band from Line 5 and Line 1 are shown in Fig. 12. Surface wave noise from ambient noise sources located near the surface and surface waves generated by passing cars in ambient noise panels from Line 1 are weaker than surface waves in ambient noise panels from Line 5.

Body-wave noise from ambient noise sources is visually identifiable on both lines (Figs 12e and f). These body waves have high apparent velocities (higher than 2000 m s^{-1}), appear in the higher-frequency band (12–26 Hz) and the individual noise bursts can be correlated to one another (Figs 12e and f). Therefore, the body-wave noise sources must be in the subsurface. In general, the body-wave noise is clearer on Line 1 than on Line 5. This suggests that it may be easier to retrieve reflected waves from the Line 1 passive data compared with Line 5. Retrieved common source gathers from Line 1 confirm this and these data were processed to obtain a stack (Fig. 13a). Processing included filtering out the surface waves and then a conventional CDP processing scheme (Table 2). A similar processing scheme was applied to the active source seismic measurements (Table 3). The active source data were filtered to approximately match the frequency content of the passive data prior to processing. It should be noted that source spacing in the active and passive measurements is different. In the active survey, source spacing is 12 m and the total number of shots is 79. In addition, source position and receiver position do not coincide. In the passive survey, the geophone spacing is 24 m. Therefore, the fold of the active survey is about twice that of the passive survey. To compensate for the difference in fold, we focused on the central parts of both surveys and included only every other source point when stacking the active source data. The resulting passive and active source stacked sections processed for the same low-frequency content are quite similar (Figs 13a and b). Fig. 13(c) shows a CDP-stacked section where only those noise panels are included in the processing that contain visually identified body-wave energy. This section along with a similar section from Line 5 (where brute force processing was not successful) is discussed in more detail later. Fig. 13(d) shows the final stacked section for the active seismic data set from Line 1 processed with the full bandwidth. The most significant reflection, K2 (Top Weser Formation), appears at approximately 500 ms in all sections and arrives at a time consistent with the 3-D seismic data (Juhlin *et al.* 2007). At about 200 ms another strong reflection is seen in all sections that corresponds to the base of the Tertiary (Juhlin *et al.* 2007). A deeper reflection is observed in the passive seismic stacked section (Fig. 13a) at about 700 ms, which is also observed in the 3-D seismic data (not shown) and the full bandwidth active seismic data. However, in the low-frequency active seismic stacked section this reflection is not obvious. Another deeper reflection appears at about 900 ms in the passive seismic stacked section (Fig. 13a) and the full bandwidth active seismic stacked section (Fig. 13d) which is consistent with a reflection observed in the low-frequency stacked section of active seismic data set (Fig. 13b). Although the passive data do not provide the resolution of the active seismic data [see Bergmann *et al.* (2011) for more results from high-resolution processing along Line 1 and Line 5] the result is encouraging.

To improve the passive imaging methodology, we applied event-driven seismic interferometry to our ambient noise data (Draganov *et al.* 2010). This approach enhances the energy of retrieved body-wave reflections and weakens the contribution of retrieved surface waves by including only ambient noise records containing identifiable body-wave arrivals in them for the seismic interferometry. As we know, the quality and characteristics of the retrieved response depends on the ambient noise present during the recording time. It has been shown that to retrieve reflected waves, one needs to suppress

Table 2. Processing steps applied to the retrieved source gathers.

Step	Parameters
1	Static correction
2	Sort to CDP domain
3	Spectral equalization
4	Velocity analysis
5	NMO (normal moveout) correction
6	Stack
7	Trace balance
8	FX-deconvolution
9	Bandpass filter

Table 3. Processing steps applied to the active data set.

Step	Parameters
1	Read and decode SEGD data
2	Create and apply geometry
3	Edit bad traces and reverse traces polarity
4	Pick first arrivals
5	Geometrical spreading compensation
6	Spectral equalization
7	Ground roll mute
8	Refraction statics
9	Sort to CDP domain
10	Velocity analysis
11	Residual statics
12	NMO correction
13	Trace balance
14	Stack
15	FX-deconvolution
16	Bandpass filter

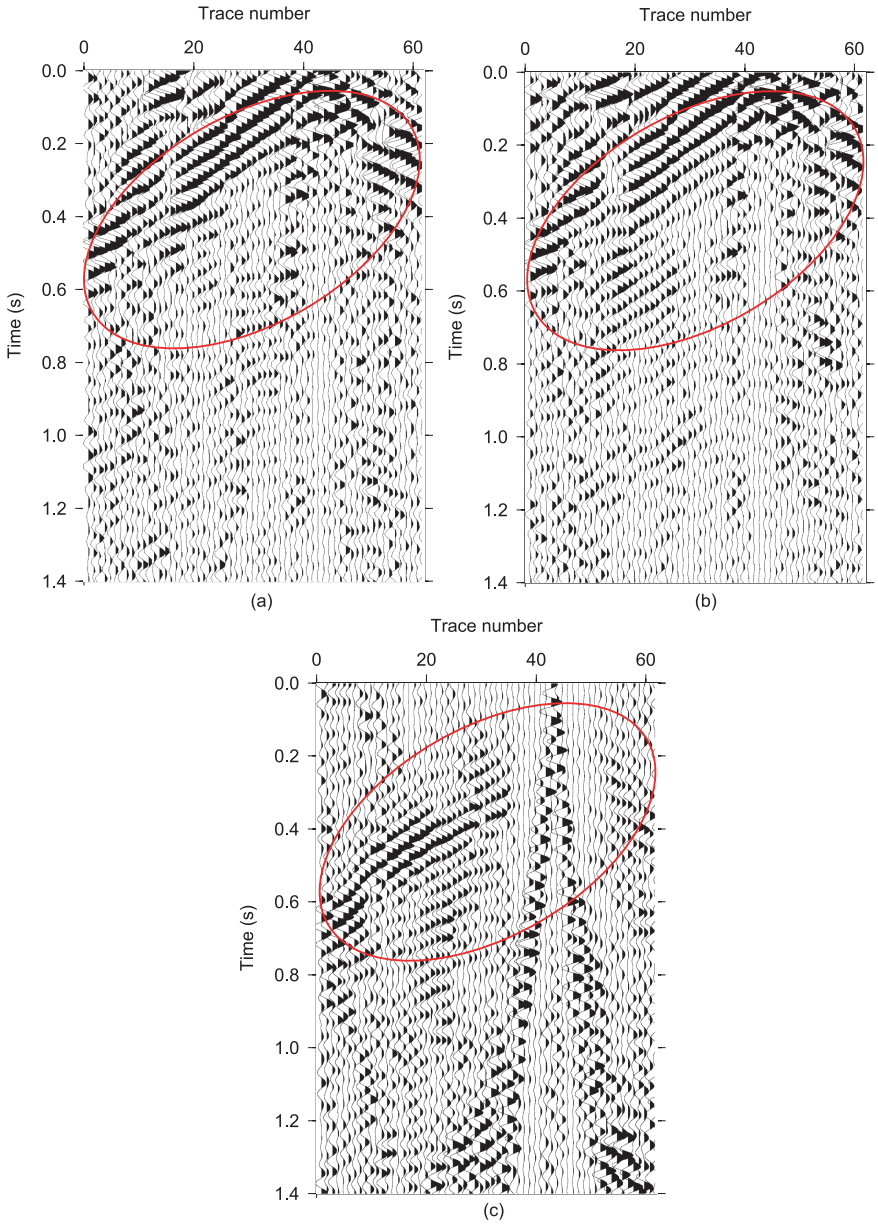

Figure 14. (a) Retrieved common source gather with the retrieved source located at the position of the 43th receiver (Line 5) using all the noise panels. The retrieved gather contains mainly body waves after spectral equalization between 12 and 26 Hz. (b) As in (a), but using noise panels containing identifiable body-wave noise. (c) Active common source gather with a source located near the same receiver position after bandpass filtering between 12 and 26 Hz.

the surface wave arrivals in the recorded ambient noise. Initially we applied a bandpass filter to do this. To further suppress the retrieval of surface waves and enhance the retrieval of reflected waves, we made a visual inspection of the ambient noise data to select those noise panels that exhibited identifiable body-wave noise; only such noise panels were then used for the seismic interferometry. In total, there are more than 4 hr of recorded noise data containing visually identifiable body-wave events from the two lines. When processing only this subset of the data, we did not use the sign-bit conversion for the retrieval of reflected waves since the quality of the retrieved reflections deteriorated if it was applied. Retrieved reflected waves are somewhat enhanced when only using the noise panels containing clear body waves for the interferometry (compare Fig. 14b with 14a). For further comparison, Fig. 14(c) shows an active source gather close to the same location as the retrieved source gathers after bandpass filtering.

The improvement in the stacked section is more dramatic when only using noise panels containing identifiable body-wave noise. We now observe reflections at 500 ms from the K2 horizon and at 200 ms from the base of the Tertiary on Line 5 (Fig. 15a), as we did on Line 1. The image is neither as good as the one from Line 1 (Fig. 13c), nor as good as the active source data processed in the same frequency band (Fig. 15b), but it is much improved over the one obtained when stacking all the data (brute force approach) in which no reflections could be identified. For comparison, Fig. 15(c) shows the resulting active source stacked section for Line 5 processed with the full bandwidth.

Based on the success we had with Line 5, we also applied the event-driven seismic interferometry to the ambient noise data from Line 1 (Fig. 13c). We found that the new stacked section exhibits better coherency of events and higher SNR compared to the results when all the recorded noise panels were used in the seismic

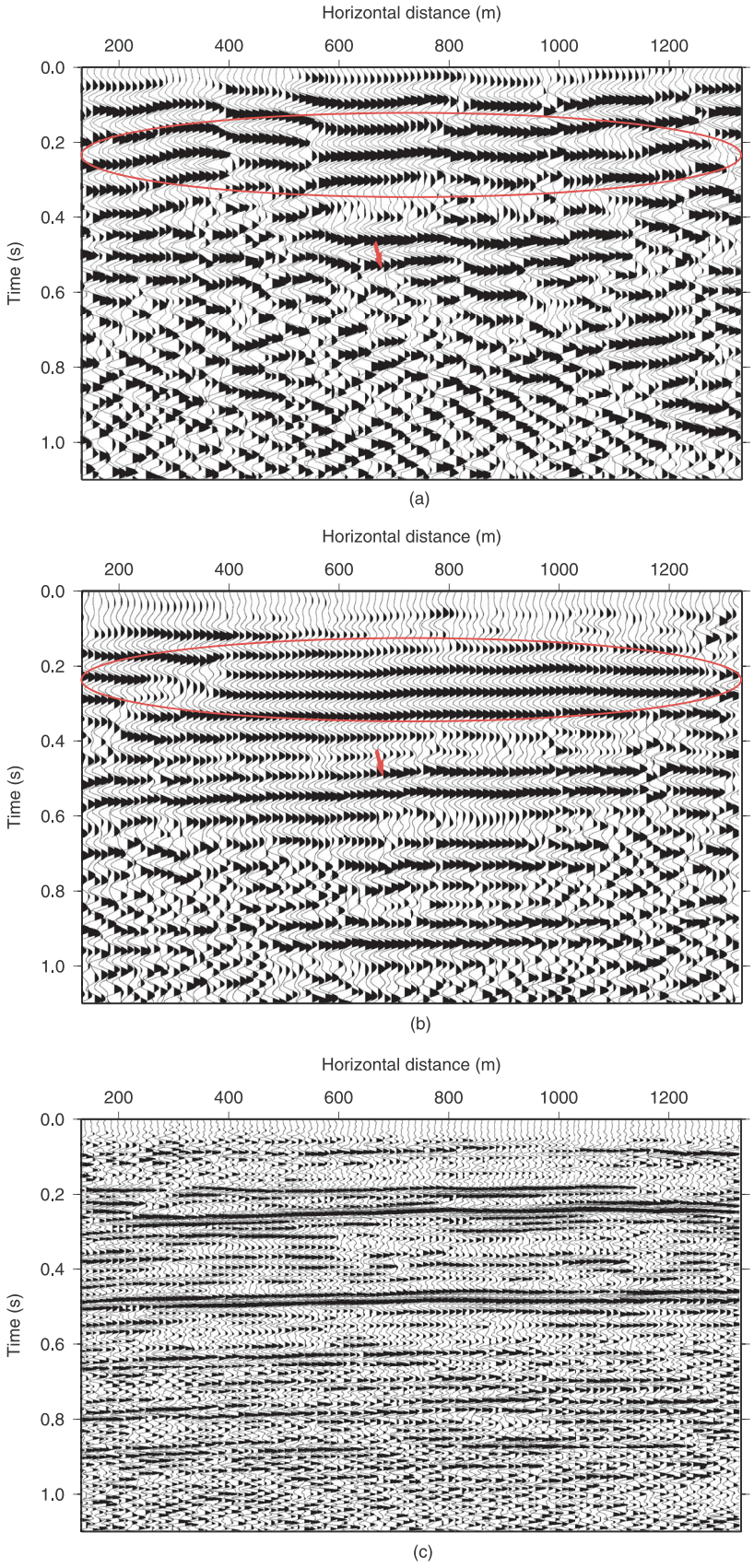

Figure 15. Stacked seismic section obtained along Line 5 from: (a) the retrieved common source gathers using noise panels containing identifiable body-wave noise from the passive measurements, (b) the common source gathers from the low frequency content of the active source survey and (c) the common source gathers from the full bandwidth active source survey.

interferometry (compare Fig. 13c with 13a). However, the retrieval of reflected waves from the deeper subsurface is not as good, due to the more limited recording time (4 instead of 25 hr). Overall, the event-driven approach applied to our ambient noise data enhances the retrieved reflections and improves the SNR of the retrieved results. A combination of the event-driven approach and a brute force approach (using all panels) may produce the optimum stacked section. Robust field methods for identifying ambient noise panels containing body waves need to be developed so that enough relevant data are recorded before finishing a survey. Almagro Vidal *et al.* (2011a,b) proposed such a method in which illumination diagnostics of recorded ambient noise are made before completing a survey. They applied the method with some success to improve the quality of the retrieved reflections. If such methods can be further developed, or permanent stations employed, then seismic ambient noise interferometry can potentially be applied to time-lapse measurements for monitoring CO_2 storage sites.

6 CONCLUSIONS

We have retrieved common source gathers by cross-correlation of ambient noise data recorded along profiles that were designed for active source surveys. For the present data set a passive recording time of about 25 hr appears to be sufficient for retrieval of surface waves. For each receiver position along the profiles, a common source gather has been retrieved. We observe surface waves, apparent refracted waves and reflected waves in the retrieved gathers. Stacking of common offset gathers into one super common source gather increases the SNR of all the wave modes. The surface waves are best observed in the frequency range 2–14 Hz and the body waves in the frequency range 12–26 Hz. Comparison with active source data shows that the retrieved surface waves and reflected waves have similar velocities and traveltimes in both data sets, confirming the validity of the passive data processing. Velocities of the retrieved apparent refracted waves at far offset are greater than those observed in the active source data, these being virtual refractions from deeper layers. CDP processing of the retrieved common source gathers from Line 1 results in a stacked section that is in reasonable agreement with that of an active source section if those data are processed with similar frequencies. If we input only noise panels containing dominant body waves for the seismic interferometry to suppress the influence of surface waves, then the retrieved reflected waves are of higher quality at early arrival times in the retrieved common source gathers. Use of this event-driven approach allowed us to image reflected waves on one of the lines (Line 5) that could not be imaged when all the data were stacked.

A surface wave dispersion curve could be estimated from the retrieved common source gathers and the stacked common offset gather. Inversion of the averaged dispersion curve results in an average (1-D) *S*-wave profile below the site that is consistent with active source data from the area, but has higher resolution in the uppermost tens of metres. In addition, 2-D velocity models obtained from first arrival traveltime tomography, where the *P*-wave velocity has been converted to *S*-wave velocity assuming a V_p/V_s ratio of 2, and surface wave dispersion curves (2-D) also show similarities. Our study shows that the retrieval of surface waves and reflected waves from ambient seismic noise by seismic interferometry may be a cheap, convenient and environmentally friendly complement to active seismic exploration. Passive seismic surveys may have a potential for seismic frontier exploration and monitoring.

ACKNOWLEDGMENTS

Seismic data acquisition was partly funded by the Geotechnologien programme of the German Federal Ministry of Education and Research, BMBF (project 3DRep1 AZ 03G0679A and CO2MAN). GLOBE ClaritasTM under license from the Institute of Geological and Nuclear Sciences Limited, Lower Hutt, New Zealand, was used to process some of the seismic data. We also appreciate Herrmann and Ammon for supplying the Computer Programs in Seismology (CPS) code. The European Commission is gratefully acknowledged for their funding of the 'CO2SINK – CO2 Storage by Injection into a Natural Storage at Ketzin', Project No. 502599. We would like to thank Deyan Draganov and one anonymous reviewer for helpful and constructive comments that improved the manuscript.

REFERENCES

Almagro Vidal, C., van der Neut, J., Draganov, D., Drijkoningen, G. & Wapenaar, K., 2011a. Retrieval of reflections from ambient noise using the incident fields (point-spread function) as a diagnostic tool, in *Proceedings of 73rd EAGE Conference and Exhibition,* Vienna (available at http://www.earthdoc.org/detail.php?pubid=50904).

Almagro Vidal, C., van der Neut, J., Draganov, D., Drijkoningen, G. & Wapenaar, K., 2011b. Retrieval of reflections from ambient-noise field data using illumination diagnostics, *SEG Expanded Abstr.,* **30,** 1613–1617, doi:10.1190/1.3627512.

Bergmann, P., Yang, C., Luth, S., Juhlin, C. & Cosma, C., 2011. Time-lapse processing of 2D seismic profiles with testing of static correction methods at the CO2 injection site Ketzin (Germany), *J. appl. Geophys.,* **75,** 124–139.

Campillo, M. & Paul, A., 2003. Long-range correlations in the diffuse seismic coda, *Science,* **299,** 547–549.

Claerbout, J.F., 1968. Synthesis of a layered medium from its acoustic transmission response, *Geophysics,* **33,** 264–269.

Daneshvar, M., Clay, C. & Savage, M., 1995. Passive seismic imaging using microearthquakes, *Geophysics,* **60,** 1178–1186.

Derode, A., Tourin, A. & Fink, M., 1999. Ultrasonic pulse compression with one-bit time reversal through multiple scattering, *J. appl. Phys.,* **85,** 6343–6352.

Dong, S., Sheng, J. & Schuster, J.T., 2006. Theory and practice of refraction interferometry, *SEG Expanded Abstr.,* **25,** 3021–3025, doi:10.1190/1.2370154.

Dorman, J. & Ewing, M., 1962. Numerical inversion of surface-wave dispersion data and crust-mantle structure in the New York-Pennsylvania area, *J. geophys. Res.,* **67,** 5227–5241.

Draganov, D., Wapenaar, K. & Thorbecke, J., 2006. Seismic interferometry: reconstructing the earth's reflection response, *Geophysics,* **71,** SI61–SI70.

Draganov, D., Wapenaar, K., Mulder, W., Singer, J. & Verdel, A., 2007. Retrieval of reflections from seismic background-noise measurements, *Geophys. Res. Lett.,* **34,** L043054, doi:10.1029/2006GL028735.

Draganov, D., Campman, X., Thorbecke, J., Verdel, A. & Wapenaar, K., 2009. Reflection images from seismic noise, *Geophysics,* **74,** A63–A67.

Draganov, D., Campman, X., Thorbecke, J., Verdel, A. & Wapenaar, K., 2010. Event-driven seismic interferometry with ambient seismic noise, in *Proceedings of 72nd EAGE Conference and Exhibition,* Barcelona (available at http://www.earthdoc.org/detail/php?pubid=39364).

Duvall, T.L., Jefferies, S.M., Harvey, J.W. & Pomerantz, M.A., 1993. Time-distance helioseismology, *Nature,* **362,** 430–432.

Forghani, F. & Snieder, R., 2010. Underestimation of body-waves and feasibility of surface-wave reconstruction by seismic interfermetry, *Leading Edge,* **29,** 796–799.

Förster, A. *et al*., 2006. Baseline characterization of the CO2SINK geological storage site at Ketzin, Germany, *Environ. Geosci.,* **13,** 145–160.

Gerstoft, P., Sabra, K., Roux, P., Kuperman, W.A. & Fehler, M., 2006. Green's functions extraction and surface-wave tomography from microseisms in southern California, *Geophysics,* **71,** SI23–SI32.

Gilles, P.M., Duvall, T.L., Scherrer, P.H. & Bogart, R.S., 1997. A subsurface flow of material from the Sun equator's to its poles, *Nature,* **390,** 52–54.

Gouedard, P. *et al*., 2008. Cross-correlation of random fields: mathematical approach and applications, *Geophys. Prospect.,* **56,** 375–393.

Gudmundsson, O., Khan, A. & Voss, P., 2007. Rayleigh-wave group-velocity of the Icelandic crust from correlation of ambient seismic noise, *Geophys. Res. Lett.,* **34,** L14314, doi:10.1029/2007GL030215.

Herrmann, R.B. & Ammon, C.J., 2002. *Computer Programs in Seismology version 3.20: Surface Waves, Receiver Functions, and Crustal Structure*, St. Louis University, Missouri.

Juhlin C., 1995. Finite difference elastic wave propagation in 2-D heterogeneous transversely isotropic media, *Geophys. Prospect.,* **43,** 843–858.

Juhlin C. *et al*., 2007. 3D baseline seismics at Ketzin, Germany: the CO2SINK project, *Geophysics,* **72,** B121–B132.

Larose E., Derode, A., Campillo, M. & Fink, M., 2004. Imaging from one-bit correlations of wide-band diffuse wavefield, *J. appl. Phys.,* **95,** 8393–8399.

Larose, E., Lobkis, O.I. & Weaver, R.L., 2006a. Passive correlation imaging of a buried scatterer, *J. acoust. Soc. Am.,* **119,** 3549–3552.

Larose, E. *et al*., 2006b. Correlation of random fields: an interdisciplinary review, *Geophysics,* **71,** SI11–SI21.

Lu, R., Venkataraman, A., Payne, M. & Zhang, J., 2009. Application of noise interferometry to obtain time-lapse velocity variations during a steam stimulation cycle at Cold Lake, *SEG Expanded Abstr.,* **28,** 1673–1677, doi:10.1190/1.3255171.

Malcolm, A., Scales, J. & Tiggelen, B., 2004. Extracting the Green function from diffuse, equipartitioned waves, *Phys. Rev. E,* **70,** 015601(R)-1–015601(R)-4.

Martens, S., Liebscher, A., Möller, F., Würdemann, H., Schilling, F., Kühn, M. & Ketzin Group, 2011. Progress report on the first European on-shore CO2 storage site at Ketzin (Germany): second year of injection, *Energy Procedia,* **4,** 3246–3253.

Mikesell, D., van Wijk, K., Calvert, A. & Haney, M., 2009. The virtual refraction: useful spurious energy in seismic interferometry, *Geophysics,* **74,** A13–A17.

Nazarian, S., Stokoe, K.H. & Hudson, W.R., 1983. Use of spectral analysis of surface waves method for determination of moduli and thicknesses of pavement systems, *Transport. Res. Record,* **930,** 38–45.

Nichols, J., Mikesell, D. & van Wijk, K., 2010. Application of the virtual refraction to near-surface characterization at the Boise Hydrogeophysical Research Site, *Geophys. Prospect.,* **58,** 1011–1021.

Nunziata, C., De Nisco, G. & Panza, G.F., 2009. S-wave profiles from noise cross correlation at small scale, *Eng. Geol.,* **105,** 3–4.

Rickett, J. & Claerbout, J., 1999. Acoustic daylight imaging via spectral factorization: helioseismology and reservoir monitoring, *Leading Edge,* **18,** 957–960.

Ritzwoller, M., Shapiro, N., Pasyanos, M., Bensen, G. & Tang, Y., 2005. Short-period surface wave dispersion measurements from ambient seismic noise in North Africa, the Middle East, and Central Asia, in *Proceedings of 27th Seismic Research Review: Ground-Based Nuclear Explosion Monitoring Technologies,* Palm Springs, CA, pp. 161–170.

Roux, P., Kuperman, W.A. & the NPAL Group, 2004. Extracting coherent wavefronts from acoustic ambient noise in the ocean, *J. acoust. Soc. Am.,* **116,** 1995–2003.

Sabra, K.G., Roux, P. & Kuperman, W.A., 2005a. Arrival-time structure of the time-averaged ambient noise cross-correlation function in an oceanic waveguide, *J. acoust. Soc. Am.,* **117,** 164–174.

Sabra, K., Gerstoft, P., Roux, P., Kuperman, W. & Fehler, M., 2005b. Extracting time-domain Green's functions from ambient seismic noise, *Geophys. Res. Lett.,* **32,** L03310, doi:10.1029/2004GL021862.

Scherbaum, F., 1987a. Seismic imaging of the site response using microearthquake recordings, Part I: method, *Bull. seism. Soc. Am.,* **77,** 1905–1923.

Scherbaum, F., 1987b. Seismic imaging of the site response using microearthquake recordings, Part II: application to the Swabian Jura, southwest Germany, seismic network, *Bull. seism. Soc. Am.,* **77,** 1924–1944.

Schuster, G.T. & Rickett, J., 2000. Daylight imaging in V(x,y,z) media, Utah Tomography and Modeling-Migration Project Midyear Report and SEP Report at Stanford University.

Shapiro, N. & Campillo, M., 2004. Emergence of broadband Rayleigh waves from correlations of the ambient seismic noise, *Geophys. Res. Lett.,* **31,** L07614, doi:10.1029/2004GL019491.

Shapiro, N., Campillo, M., Stehly, L. & Ritzwoller, M., 2005. High-resolution surface-wave tomography from ambient seismic noise, *Science,* **307,** 1615–1618.

Sheng, J., Schuster, G.T. & Nowack, R., 2001. Imaging of crustal layers by teleseismic ghosts, *EOS, Trans. Am. geophys. Un.,* **82,** Fall Meet. Supp., Abstract S32C–0658.

Sheng, J., Schuster, G.T., Pankow, K., Pechmann, J. & Nowack, R., 2003. Coherence-weighted wavepath migration of teleseismic data, *EOS, Trans. Am. geophys. Un.,* **84,** Fall Meet. Supp., Abstract S11E–0344.

Shragge, J., Artman, B. & Wilson, C., 2006. Teleseismic shot-profile migration, *Geophysics,* **71,** SI221–SI229.

Snieder, R., 2004. Extracting the Green's function from the correlation of coda waves: a derivation based on stationary phase, *Phys. Rev. E,* **69,** 046610, doi:10.1103/PhysRevE.69.046610.

Wapenaar, K., 2004. Retrieving the elastodynamic Green's function of an arbitrary inhomogeneous medium by cross correlations, *Phys. Rev. Lett.,* **93,** 254301-1–254301-4.

Wapenaar, K. & Fokkema, J., 2006. Green's function representations for seismic interferometry, *Geophysics,* **71,** SI33–SI46.

Wapenaar, K. & Snieder, R., 2007. From order to disorder to order: a philosophical view on seismic interferometry, *SEG Expanded Abstr.*, **26,** 2683–2687, doi:10.1190/1.2793024.

Weaver, R.L. & Lobkis, O.I., 2001. Ultrasonics without a source: thermal fluctuation correlations at MHz frequencies, *Phys. Rev. Lett.,* **87,** 134301-1–134301-4.

Weaver, R.L. & Lobkis, O.I., 2003. Elastic wave thermal fluctuations, ultrasonic waveforms by correlation of thermal phonons, *J. acoust. Soc. Am.,* **113,** 2611–2621.

Weaver, R.L. & Lobkis, O.I., 2004. Diffuse fields in open systems and the emergence of the Green's function, *J. acoust. Soc. Am.,* **116**(5), 2731–2734.

Yang, C., Juhlin, C., Enescu, N., Luth, S. & Cosma, C., 2010. Moving Source Profile (MSP) data processing, modeling and comparison with 3D surface seismic data at the C02SINK project site, Ketzin, Germany, *Near Surf. Geophys.,* **8,** 601–610.

Yao, H., van der Hilst, R.D. & de Hoop, M.V., 2006. Surface-wave array tomography in SE Tibet from ambient seismic noise and two-station analysis: I—phase velocity maps, *Geophys. J. Int.,* **166,** 732–744.

Yordkayhun, S., Giese, R., Juhlin, C. & Cosma, C., 2007. Shallow velocity-depth model using first arrival traveltime inversion at the CO2SINK site, Ketzin, Germany, *J. appl. Geophys.,* **63,** 68–79.

Yordkayhun, S., Juhlin, C. & Norden, B., 2009a. 3D seismic reflection surveying at the CO2SINK project site, Ketzin, Germany: a study for extracting shallow subsurface information, *Near Surf. Geophys.,* **7,** 75–91.

Yordkayhun, S., Tryggvason, A., Norden, B., Juhlin, C. & Bergman, B., 2009b. 3D seismic traveltime tomography imaging of the shallow subsurface at the CO2SINK project site, Ketzin, Germany, *Geophysics,* **74,** G1–G15.